

SAR tomography as an add-on to PSI for improved deformation sampling in urban areas: A quality assessment

Muhammad Adnan Siddique^{*1}, Urs Wegmüller², Irena Hajnsek^{1,3}, Othmar Frey^{1,2}

¹Earth Observation & Remote Sensing, ETH Zurich, Switzerland

²Gamma Remote Sensing, Gümligen, Switzerland

³Microwaves & Radar Institute, Oberpfaffenhofen, German Aerospace Center – DLR, Germany

*Email: siddique@ifu.baug.ethz.ch

Abstract

Persistent scatterer interferometry (PSI) typically rejects layovers. Therefore, layover-affected urban areas may suffer from inadequate deformation sampling. SAR tomography, when used as an add-on to PSI, reveals additional deformation samples by resolving layovers. In this paper we quantify the relative gain in deformation sampling, while taking into account the quality of the additional (double) scatterers in terms of root-mean-square (RMS) phase deviation. We experiment on an interferometric stack of 50 TerraSAR-X stripmap images acquired over the city of Barcelona. The results show a tradeoff between the gain and the quality of the detected scatterers. For the observed urban area, we obtain a gain of 9.8% while the RMS phase deviation for 99% of the detected double scatterers is less than 1.1 radians.

1 Introduction

Persistent scatterer interferometry (PSI) [1, 2] is in operational use as a tool for spaceborne deformation monitoring with SAR sensors. In urban areas, PSI generally provides good coverage in terms of the spread and quantity of the persistent scatterers (deformation samples). However, an inherent limitation associated with PSI techniques is that the pixels containing multiple scatterers, as for the case of a layover, are typically rejected. Therefore, layover-affected areas may suffer from inadequate deformation sampling. SAR tomography [3, 4, 5] has the ability to overcome this limitation by resolving layovers. While classical SAR tomographic methods only allow layover separation along the elevation, advanced differential tomographic methods with extended phase models [6, 7, 8, 9] additionally allow estimating the deformation parameters of the individual scatterers overlaid in the same pixel. In this way, SAR tomography not only resolves the layover but serves to improve the deformation sampling in the observed area.

In the context of operationally combining SAR tomography with a PSI approach [10, 8], it is pertinent to quantitatively assess the relative gain in deformation sampling offered by the added use of tomography. At the same time, the quantity of the scatterers obtained with tomography needs to be weighed against their *quality*. Furthermore, in order that the improvement in deformation sampling with tomography is meaningful, the quality of the scatterers obtained with tomography should be comparable to the quality of the persistent scatterers obtained with a PSI approach. To address the aforementioned concerns, we adopt the following approach in this paper. First, we perform a PSI analysis of an urban area using the Interferometric Point Target Analysis (IPTA) [2] on an interferometric data stack comprising of stripmap images. A set

of PSs is iteratively identified. The PSI solution obtained comprises of the estimates of residual height, linear deformation velocity and phase-to-temperature [11] sensitivity of each PS. The atmospheric phase screen (APS) is isolated within the IPTA processing. The data stack is phase calibrated by subtracting the APS (after extrapolation over the entire scene) from the interferograms. Next, we implement single-look tomographic inversion on the phase calibrated data stack with an extended phase model that simultaneously models scatterer elevation, linear deformation as well as thermal dilation [8]. Tomographic inversion is applied on all pixels, including the pixels rejected during the IPTA processing which potentially include double scatterers. A generalized likelihood ratio test (GLRT) [12] is used for the detection of single and double scatterers. The quality of the detected scatterers (DSs) is assessed in terms of the residual phase in each layer, and compared against the quality of the PSs obtained with IPTA processing. The relative gain in deformation sampling is quantitatively assessed vis-a-vis the corresponding quality of the detected scatterers.

2 SAR Tomography

2.1 Mathematical Model

The mathematical model for advanced SAR tomography that simultaneously models scatterer elevation, deformation and thermal dilation can be written as [9, 8]:

$$y_n = \iiint_{\Delta s, \Delta \nu, \Delta \kappa} \gamma(s, \nu, \kappa) \exp[-j\varphi_n(s, \nu, \kappa)] ds d\nu d\kappa \quad (1)$$

where y_n is the SLC value for a given range-azimuth pixel in the n^{th} layer of the interferometric stack, for $n = 0, 1, \dots, N - 1$. $\gamma(s, \nu, \kappa)$ is the target reflectiv-

ity as a function of the scatter elevation s , linear deformation velocity ν , and phase-to-temperature sensitivity κ [11]. Δs , $\Delta \nu$ and $\Delta \kappa$ represent the observed extents of s , ν and κ , respectively. The interferometric phase is modeled as follows:

$$\varphi_n(s, \nu, \kappa) = 2k \left[\Delta r_n(s) + \nu t_n + \frac{1}{2k} \kappa \tau_n \right] \quad (2)$$

where $\Delta r_n(s)$ is the sensor-to-target path-length difference for the interferometric pair, t_n is the n^{th} temporal baseline and τ_n is the temperature change for the n^{th} layer relative to the reference layer $n = 0$.

$$\Delta r_n(s) = r_n(s) - r_0(s) \approx \frac{s^2}{2(r_0 - b_n^{\parallel})} - \frac{b_n^{\perp} s}{r_0 - b_n^{\parallel}}. \quad (3)$$

The range distance from sensor n to the scatterer at elevation s is represented by r_n . The orthogonal and parallel components of the n^{th} spatial baseline are b_n^{\perp} and b_n^{\parallel} , respectively. The phase model in eq. 2 assumes that the scatterer deformation consists of two forms of motion – a temporally linear line-of-sight (LOS) displacement over the entire time series, and a temperature-dependent LOS dilation due to the thermal expansion of building structures [11, 8].

2.2 Tomographic Inversion & Scatterer Detection

Considering that a given range-azimuth pixel has not more than two temporally coherent scatterers, we make the following hypotheses: \mathcal{H}^0 – the pixel does not represent a stable scatterer; \mathcal{H}^1 – the pixel is a single scatterer, or \mathcal{H}^2 – the pixel is a double scatterer. Let \mathbf{p} be the vector of the unknown scatterer parameters: $\mathbf{p} = [s, \nu, \kappa]$. Assuming the presence of at least one temporally coherent scatterer in a given pixel, we estimate the parameters of the first scatterer, \mathbf{p}_1 with the following beamforming-based optimization:

$$\hat{\mathbf{p}}_1 = \arg \max_{\mathbf{p}} (|\mathbf{a}^H(\mathbf{p}) \mathbf{y}|) \quad (4)$$

where \mathbf{y} is the SLC vector and $\mathbf{a}(\mathbf{p})$ is the steering vector:

$$\mathbf{a}(\mathbf{p}) = [1 \quad e^{-j\varphi_1(\mathbf{p})} \quad \dots \quad e^{-j\varphi_{N-1}(\mathbf{p})}]^T. \quad (5)$$

The parameters for a potential second scatterer, $\hat{\mathbf{p}}_2$ are computed by applying the following beamforming-based maximization [12]:

$$\mathbf{p}_2 = \arg \max_{\mathbf{p}} \left(\frac{|\mathbf{a}^H \mathbf{y}_c|^2}{\|\mathbf{y}_c\|^2} \right) \quad (6)$$

where $\mathbf{y}_c = \mathbf{P}_1^{\perp} \mathbf{y}$ and $\hat{\mathbf{P}}_1^{\perp} = \mathbf{I}_N - \frac{\mathbf{a}(\hat{\mathbf{p}}_1) \mathbf{a}^H(\hat{\mathbf{p}}_1)}{N}$.

To distinguish between the hypotheses \mathcal{H}^0 , \mathcal{H}^1 , and \mathcal{H}^2 , we use the *sequential generalized likelihood ratio*

test with cancellation (SGLRTC), as proposed in [12]. SGLRTC first checks whether a given pixel is a double-scatterer as follows:

$$\left(\frac{|\mathbf{u}_c^H \mathbf{y}_c|^2}{\|\mathbf{y}_c\|^2} \right) \underset{\mathcal{H}^2}{\overset{\mathcal{H}^2}{\gtrless}} T_2 \quad (7)$$

where $\mathbf{u}_c = \hat{\mathbf{P}}_1^{\perp} \mathbf{a}(\hat{\mathbf{p}}_2) / \|\hat{\mathbf{P}}_1^{\perp} \mathbf{a}(\hat{\mathbf{p}}_2)\|$ and $\mathbf{y}_c = \hat{\mathbf{P}}_1^{\perp} \mathbf{y}$. In case the hypothesis \mathcal{H}^2 is rejected, a decision is made between \mathcal{H}^0 and \mathcal{H}^1 as follows:

$$\left(\frac{|\mathbf{a}^H(\hat{\mathbf{p}}_1) \mathbf{y}|^2}{N^2 \|\mathbf{y}\|^2} \right) \underset{\mathcal{H}^0}{\overset{\mathcal{H}^1}{\gtrless}} T_1. \quad (8)$$

As suggested in [12], we set the thresholds at the same value to jointly maximize the probabilities of detection for both the single and double scatterers for a given probability of false alarm.

2.3 Quality in terms of Phase Residue

We assess the quality of the estimates obtained from the tomographic model by means of the root-mean-square (RMS) phase deviation (as it is done in the IPTA processing). Using the estimated parameters, we compute the estimated SLC vector, \mathbf{y}_{est} (model fit) as follows:

$$\mathbf{y}_{est} = \begin{cases} \hat{\gamma}_1 \mathbf{a}(\hat{\mathbf{p}}_1) & \text{single scatterer} \\ \hat{\gamma}_1 \mathbf{a}(\hat{\mathbf{p}}_1) + \hat{\gamma}_2 \mathbf{a}(\hat{\mathbf{p}}_2) & \text{double scatterer} \end{cases} \quad (9)$$

where $\hat{\gamma}_1$ and $\hat{\gamma}_2$ are the estimated reflectivities of the first and second scatterer, respectively: $\hat{\gamma}_1 = \mathbf{a}^H(\hat{\mathbf{p}}_1) \mathbf{y}$ and $\hat{\gamma}_2 = \mathbf{a}^H(\hat{\mathbf{p}}_2) \mathbf{y}_c / \|\hat{\mathbf{P}}_1^{\perp} \mathbf{a}(\hat{\mathbf{p}}_2)\|$. The phase deviation for the n^{th} layer, φ_n^{res} is computed as the angle difference between the phases of y_n and $y_{n,est}$. Low phase deviations represent a better fit of the tomographic model to the measurements. The RMS phase deviation, $\sigma_r^{tomo} = \sqrt{\frac{1}{N-1} \sum_{n=1}^N (\varphi_n^{res})^2}$ is used as a metric for the goodness of fit, and hence as a metric for the quality of the scatterers.

2.4 Relative Gain in Deformation Sampling

We define the gain in deformation sampling, G achieved by using SAR tomography relative to a PSI-based analysis of a given area as follows:

$$G = \left(\frac{2N_{d,u} + N_{d,ps}}{N_{psi}} \right) \times 100\%. \quad (10)$$

$N_{d,u}$ is the number of pixels that are uniquely detected as double scatterers, i.e. the pixels were not identified as PSs in the IPTA processing. $N_{d,ps}$ is the number of those pixels that are detected as double scatterers but were also identified as PSs, and N_{psi} is the total number of PSs.

3 Results

We conduct this investigation on an interferometric stack of 50 TerraSAR-X stripmap images acquired over a time span of nearly 5 years. The test site is an urban area in the city of Barcelona, Spain, as shown in Fig. 1. We first perform a PSI analysis using IPTA [2]. Fig. 1 shows the estimated linear deformation velocity for the PSs identified in the IPTA processing. Single-look beamforming-based tomographic inversion is applied next. Using the scatterer parameters estimated with tomography, an implementation following the SGLRTC approach [12] is used to detect single and double scatterers. Fig. 2 shows the variation in the number of single and double scatterers detected at various thresholds, and the corresponding relative gain in deformation sampling. The number of detected scatterers generally increases with decreasing thresholds. Fig. 3 shows the distribution of the RMS phase deviation for the single and double scatterers at different thresholds. Fig. 4 shows the scatterers projected on 3D building models in Google Earth for $T_1 = T_2 = 0.4$.

4 Discussion

During the IPTA processing, the RMS phase deviation, σ_r^{ipta} is used as an indicator of the quality of each PS candidate. In our work, we used a threshold of 1.1 rad for σ_r^{ipta} , i.e. the candidates with σ_r^{ipta} higher than 1.1 rad have been rejected. For the PSs in the final solution, as shown in Fig. 1, σ_r^{ipta} is 0.57 rad on average. SAR tomography allows increasing the deformation sampling with layover separations, but it needs to be assessed whether the scatterers obtained with tomography have a quality comparable to the quality of the PSs identified in IPTA. We apply tomographic inversion and scatterer detection with SGLRTC [12] on the entire scene. Fig. 2 shows that decreasing the thresholds generally increases the quantity of the detected scatterers. For thresholds below 0.3, we observe an irregularity in the trend: there is a sudden jump in the number of double scatterers with almost no change in the number of single scatterers. This effect can be explained in terms of the decision strategy adopted in SGLRTC which first decides whether a given pixel is a double scatterer. If the threshold T_2 is too low, many potential single scatterers or simply noise would be falsely classified as double scatterers before being explicitly tested as single scatterers. Therefore, in our case, it is appropriate to choose thresholds higher than 0.3. For thresholds between 0.3-0.4, we have nearly twice as many scatterers detected with tomography than the PSs obtained with IPTA, and the relative gain, G varies between 22-9.8%. The gain declines sharply as the thresholds are increased. A suitable choice of the thresholds should also account for the quality of the scatterers. The distributions of the σ_r^{tomo} for the single and double scatterers obtained with tomography are shown in Fig. 3. For the case of single scatterers, it can be clearly seen that progressively increasing the thresholds tends to reject points of relatively lower quality.

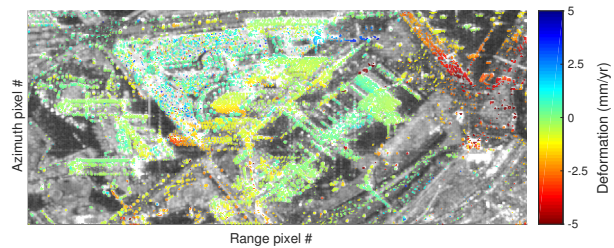


Figure 1: Average SAR backscatter image of Diagonal Mar, Barcelona. The colored dots on the image are the PSs identified in IPTA processing; the color represents linear deformation velocity.

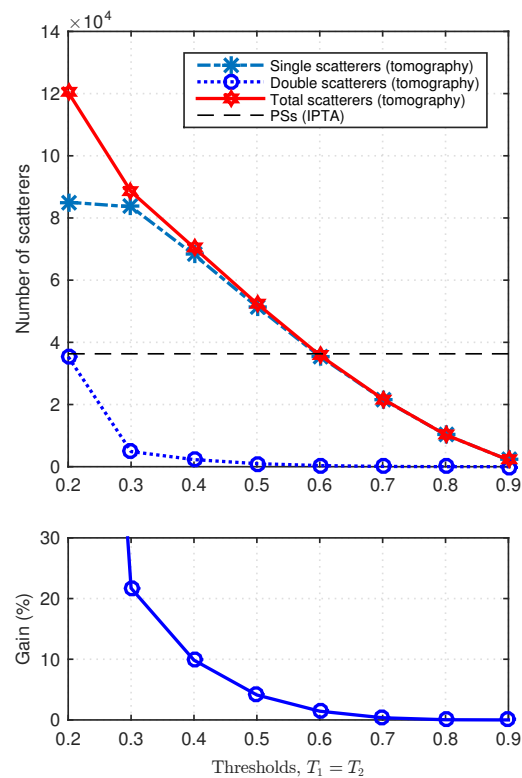


Figure 2: Top: Number of scatterers obtained with tomographic inversion versus the thresholds of detection, T_1 and T_2 , keeping $T_1 = T_2$. Below: The corresponding relative gain in the deformation sampling.

In order that the quality of these scatterers is on a par with the quality of the PSs identified in the PSI processing, we require thresholds greater than 0.5. However, for thresholds above 0.5, we see a very few double scatterers and the relative gain is merely 4% or less. In case of double scatterers, the effect of progressively increasing the thresholds on the average quality is not as pronounced as it is for the single scatterers. This is not unexpected since the phase residue for a double scatterer depends on the inversion of both the first and the second scatterer. It could be that the second scatterer suffers from phase noise leading to poor inversion; a high value of T_2 may reject it as a double-scatterer although it may still exhibit a relatively low σ_r^{tomo} due to a possibly good inversion of the first scatterer. We set $T_1 = T_2 = 0.40$ for which more than 99% of the detected double scatterers have σ_r^{tomo} less than 1.1 rad, with a relative gain of 9.8%, while the average σ_r^{tomo} for single and double scatterers is 0.69 rad and 0.66, respectively.

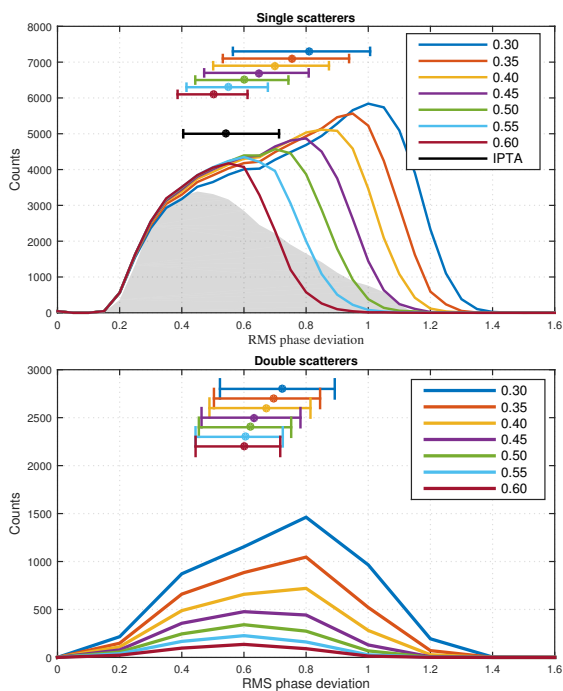


Figure 3: Distribution of the root-mean-square (RMS) phase deviation for the single (top) and double (below) scatterers obtained with tomography, at different detection thresholds (shown in different colors). The deviation bars show the interquartile range around the median.

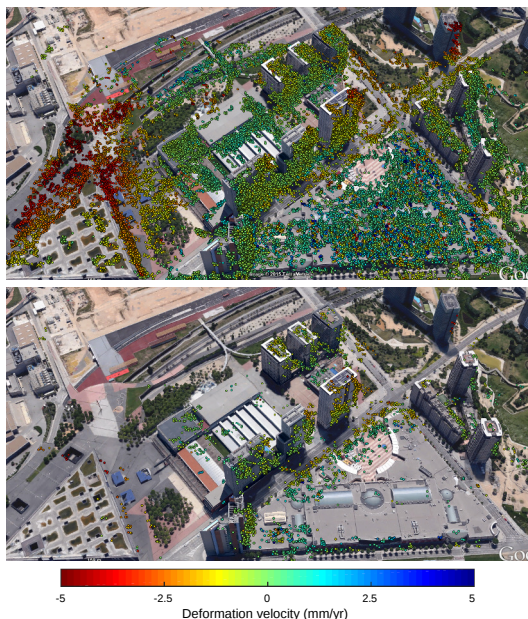


Figure 4: Single (top) and double scatterers (below) obtained with tomography for $T_1 = T_2 = 0.4$. The colors represent the estimated LOS linear deformation velocity.

5 Conclusion

In this paper, we have assessed the quality of a single-look beamforming based tomographic parameter estimation and scatterer detection in terms of RMS phase deviation, and have compared it with its PSI (IPTA) counterpart. The corresponding gain in deformation sampling through layover separations is quantitatively analyzed. The results show that the thresholds of detection required such that the quality of the single scatterers is comparable

with the quality of the PSs identified in the PSI analysis, may become too restrictive to allow for the detection of a reasonable number of double scatterers. Therefore, the choice of the thresholds has to be made as a compromise between the quality and the relative gain in deformation sampling. For our test site, setting thresholds at 0.4 allows us to have a gain of 9.8% while 99% of the double scatterers have RMS phase deviation below the upper limit of 1.1 rad set in the PSI processing.

References

- [1] A. Ferretti, C. Prati, and F. Rocca, "Permanent scatterers in SAR interferometry," *IEEE Trans. on Geosc. and Remote Sens.*, vol. 39, no. 1, pp. 8–20, 2001.
- [2] C. Werner, U. Wegmüller, T. Strozzi, and A. Wiesmann, "Interferometric point target analysis for deformation mapping," in *Proc. IEEE Int. Geosci. Remote Sens. Symp.*, 2003, pp. 4362–4364.
- [3] O. Frey and E. Meier, "3-D time-domain SAR imaging of a forest using airborne multibaseline data at L- and P-bands," *IEEE Trans. on Geosc. and Remote Sens.*, vol. 49, no. 10, pp. 3660–3664, 2011.
- [4] G. Fornaro, F. Lombardini, and F. Serafino, "Three-dimensional multipass SAR focusing: Experiments with long-term spaceborne data," *IEEE Trans. Geosci. Remote Sens.*, vol. 43, no. 4, pp. 702–714, April 2005.
- [5] A. Reigber and A. Moreira, "First demonstration of airborne SAR tomography using multibaseline L-Band data," *IEEE Trans. Geosci. Remote Sens.*, vol. 38, no. 5, pp. 2142–2152, 2000.
- [6] F. Lombardini, "Differential tomography: A new framework for SAR interferometry," *IEEE Trans. Geosci. Remote Sens.*, vol. 43, no. 1, pp. 37–44, 2005.
- [7] X. Zhu and R. Bamler, "Superresolving SAR tomography for multidimensional imaging of urban areas: Compressive sensing-based TomoSAR inversion," *IEEE Signal Process. Mag.*, vol. 31, no. 4, pp. 51–58, 2014.
- [8] M. Siddique, I. Hajnsek, U. Wegmüller, and O. Frey, "Towards the integration of SAR tomography and PSI for improved deformation assessment in urban areas," in *FRINGE Workshop*, 2015.
- [9] D. Reale, G. Fornaro, and A. Pauciuolo, "Extension of 4-D SAR imaging to the monitoring of thermally dilating scatterers," *IEEE Trans. Geosci. Remote Sens.*, vol. 51, no. 12, pp. 5296–5306, 2013.
- [10] O. Frey, M. Siddique, I. Hajnsek, U. Wegmüller, and C. Werner, "Combining SAR tomography and a PSI approach for high-resolution 3-D imaging of an urban area," in *Proc. 10th European Conf. on SAR*, 2014, pp. 1045–1048.
- [11] U. Wegmüller and C. Werner, "Mitigation of thermal expansion phase in persistent scatterer interferometry in an urban environment," in *Proc. Joint Urban Remote Sens. Event*, March 2015, pp. 1–4.
- [12] A. Pauciuolo, D. Reale, A. De Maio, and G. Fornaro, "Detection of double scatterers in SAR tomography," *IEEE Trans. Geosci. Remote Sens.*, vol. 50, no. 9, pp. 3567–3586, 2012.